Dynamics of droplets of biological fluids over enhanced surfaces with and without electrostatic actuation

J. A. Ramos[1,2], A. S. Moita*[1], D. M. F. Prazeres[2], A. L. N. Moreira[1]
[1]IN+, Center for Innovation, Technology and Policy Research, Dep. Mechanical Engineering, Instituto Superior Técnico, Universidade de Lisboa, Portugal
[2]IBB, Institute for Biotechnology and Bioengineering, Center for Biological and Chemical Engineering, Dep. Bioengineering, Instituto Superior Técnico, Universidade de Lisboa, Portugal
*Corresponding author: anamoita@dem.ist.utl.pt

Abstract
This study aims at characterizing the dynamic behaviour of droplets of biological samples over enhanced surfaces with and without electrostatic actuation, in the context of the development of a surface microfluidic chip for sample handling in lab-on-a-chip applications. The best performing enhanced surfaces are chosen based on the characterization of wettability (static and dynamic contact angles) and on the analysis of droplet impact at small velocities. Evaluating droplet impact is also used to identify and characterize non-Newtonian behaviour of the biological fluids used here.
The tests consider the use of 2-3μL droplets of sodium chloride (NaCl), bovine serum albumin (BSA) and blood plasma mock (100mmol/l NaCl, 1.2mmol/l BSA, 5.6mmol/l glucose) solutions with different concentrations. The results show a mild promotion of droplet motion by electrowetting when the concentration of the studied solutes (NaCl, BSA, glucose) was slightly increased. The apparent high saturation angle observed in the static characterization of the electowetting of BSA solutions, which might cause a limitation in their transportation and handling is suggested to be caused by the adsorption of the molecules on the dielectric substrate, which may induce modifications of the local wettability if the droplet stays in contact with the substrate for sufficient time.
Analysis of the absorption spectra before and after electrowetting reveals that BSA remains unchanged after electrostatic actuation, but that the droplet partially evaporates causing an increase on the concentration of BSA. This effect can be a problem for applications in lab-on-a-chip devices, particularly for diagnostic purposes which rely on the detection of solutes like proteins and therefore deserves more attention in future studies.

Introduction

Droplet-based transport phenomena driven by surface tension have been explored as an automated pumping source for various chemical and biological applications. Recently, researchers (e.g. [1]) have suggested an alternative microfluidic approach to create fluidic pathways using hydrophobic or superhydrophobic patterns in an open surface configuration, referred to as surface microfluidics. Indeed, control of the fluid motion at the microscale via tailoring of surface tension is advantageous, as it does avoids many eletromechanical parts, given that within this scale, surface tension forces become dominant over pressure and body forces. Local modification of the surface tension can be then obtained by a variety of methods, such as electrostatic actuation. This method is actually considered as the backbone of digital microfluidics [2] and its potential for transport and manipulation of biological fluids is pointed out by many authors. Some of these applications include DNA and protein analysis as well as biomedical diagnostics (*e.g.* [3-5]). Digital microfluidics for cell assays is also argued to be advantageous when compared to the currently used techniques [6-7]. However, most of the devices developed so far are based on continuous flow through closed channels [8]. Such closed configuration is the easiest to implement, but has several limitations associated to clogging and cleaning issues and difficulties in having access to the samples. The alternative is a single plate open configuration system [9], which brings many challenges in terms of the arrangement of the chip. Here, surface modification has a vital role, but also introduces additional complexity to the system, as the study of the wettability and electrowetting over micro-and-nano-structured surfaces often cause asymmetries in droplet shape (due to hysteresis [10]) and particular droplet morphologies which may not be stable [8]. Hence, although this open configuration has great potential for bioengineering and biomedical applications, as recently reviewed in [11], much research is still required for the production of commercially viable systems. The traditional concept of EWOD – electrowetting on dielectric, stands on the reduction of the dielectric-liquid interfacial energy by the application of a voltage between a conducting droplet and an underlying dielectric layer. The dielectric layer was introduced by Berge [12], simply to

avoid the problem of water electrolysis, which occurs at just a few hundred millivolts. Contrasting to the most current models, which consider the decrease of the contact angle as the governing effect of electrowetting controlled droplet motion, electromechanical [10,13] and energy minimization models [8,14] show that the energy gradient is in fact the driving effect behind electrowetting induced motion.
Although few authors report the successful electrowetting-induced transport of proteins, DNA and even physiological fluids [15-18], the transport phenomena seem to be affected by the adsorption of the biomolecules. Although electrochemical properties of these samples are suggested to be able to alter the transport of the microdroplets and to affect the value of the saturation angle, due to local modification and/or divergence of the electric fields near the contact line, very little research is yet reported which tries to address these issues.
Many biological samples have non-Newtonian properties. For instance, blood is known to be shear-thinning and therefore its viscosity can be well described by $\mu = K\dot{\gamma}^{n-1}$. Modifications of the values of the consistency coefficient *K* and of the power-law index *n* are suggested to be correlated with leukaemia [19]. Also, DNA can be sensitive to shear and therefore DNA samples are related in some studies to power law fluids [20]. On the other hand, although blood plasma has been reported to mainly depict a Newtonian behaviour in shear, viscoelastic characteristics may be observed in elongational flows [21]. Hence, the non-Newtonian nature of the biological fluids must be well determined and characterized.
In line with this, the present work aims at characterizing the dynamic behaviour of droplets of biological samples, such as DNA solutions and mock blood plasma solutions over enhanced surfaces with and without electrostatic actuation in the context of the development of a surface microfluidic chip for the transport of these fluids. The best performing enhanced surface is chosen based on the characterization of wettability (static and dynamic contact angles) as well as on the analysis of droplet impact at small velocities. Evaluating droplet impact will also be useful to identify and characterize non-Newtonian behaviour of the biological fluids used here. The results obtained will be compared with models reported in the literature for Newtonian and non-Newtonian fluids, as well as with our own results, partially presented in a previous work [22]. For comparative purposes, one will also analyse the behaviour of droplets of NaCl solutions with different concentrations. Afterwards, the static and dynamic angles are characterized under electrostatic actuation. This information is complemented with the dynamic analysis of the contact line motion (inducing droplet spreading) under electrostatic actuation, following the procedure reported in [23].

Material and methods

The experimental set-up is mounted on an optical tensiometer (THETA, from Attesion), so that all the droplet formation system can be controlled by the computer. For this stage of the research, large droplets with initial diameter ranging between 2.4 μm < D_0 < 3.3 mm are used to assure a good spatial accuracy of the measurements, which is vital for the precise description of the main fundamental quantities that are being investigated. For electrowetting tests the droplets are deposited on the enhanced surfaces. In the absence of electrostatic actuation the spreading is forced through impact over the surfaces with velocities U_0 ranging from 0.88 to 3m/s. As aforementioned in the Introduction, the experiments addressing droplet impact are performed to choose the best performing surfaces, i.e. those rendering the most hydrophobic behaviour for the largest number of biological samples. This initial study without electrostatical actuation is also used to discuss the Newtonian vs non-Newtonian behaviour of the biological fluids used in the present study.

All the tests are performed inside a Perspex chamber saturated with the working fluid at room temperature. This chamber has four 55x55mm^2 quartz windows to avoid distortion which introduces errors in the image based techniques.

The enhanced surfaces are made from a silicon wafer and are micro-patterned using square structural pillars, ranging from 5μm up to 200μm. Additional superhydrophobic surfaces made from aluminum and Teflon are also used. Surface topography is characterized using a Dektak 3 profile meter (Veeco) with a vertical resolution of 200Angstroms. All the surfaces are checked by SEM/EDS analysis. Table 1 summarizes the topographical characteristics of the enhanced surfaces. The main dimensions defining the micro-patterns are identified in Figure 1. For the superhydrophobic aluminum and Teflon (PTFE – polytetrafluoroethylene) surfaces, which depict a stochastic roughness profile, surface topography was quantified by the mean roughness (determined according to standard BS1134) and by the mean peak-to-valley roughness (determined following standard DIN4768), as performed in previous work (*e.g.* [24-26]).

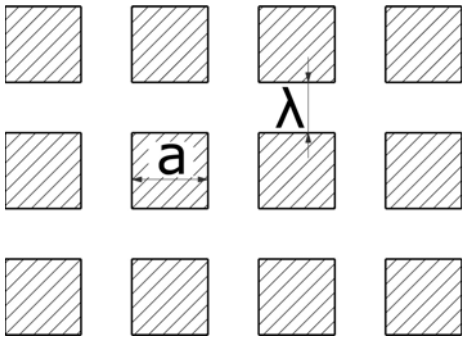

Figure 1. Schematic showing the definition of the dimensions *a* and λ characterizing the topography of the surfaces micro-structured with regular patterns.

Table 1. Surface topography and wettability with water of the surfaces used in the present study. Here *a* is the size of the side of the square cross section, h_R is the height of the squared pillars and λ is the pitch.

Surfaces	Material	Surface number	*a* μm]	h_R [μm]	λ [μm]	R_a [μm]	R_z [μm]
Smooth	Silicon wafer	S1	-	-	-	~0	~0
Structured w/regular patterns	Silicon wafer 9	S2	134	23	171	-	-
	Silicon wafer 10	S3	173	23.4	112	-	-
	Silicon wafer 14	S4	158	23.1	132	-	-
Structured w/stochastic profile	Grafted aluminum	S5	-	-	-	4.2	8
	PTFE	S6	-	-	-	~0	~0

The wettability is quantified by the static qe and dynamic qd contact angles measured using the optical tensiometer. The fluids used here are water (for control), water + xanthan gum mixtures at different wt% concentration of the gum (namely 0.05%, 0.10%, 0.15% and 0.35%), plasma mock (100mmol/l NaCl, 1.2mmol/l BSA, 5.6mmol/l glucose), DNA (0.1mM and 1mM), NaCl (with concentrations of 50mM, 100mM, 200mM and 400mM) and BSA (with concentrations of 1mM, 2.5mM - the typical concentration in blood plasma- and 50mM) solutions.

The contact angles were measured at room temperature (ca. 25°C) for all the liquid/surface pairs considered in the present study using the optical tensiometer THETA (Attension). Four to five consistent measures were taken for each sample using the sessile drop method. Images of the deposited droplet were taken using a monochrome video-camera coupled with a microscope. The images size is 640×480 pixels and the spatial resolution of the system for the current optical configuration is 15.6 μm/pixel. The images were post-processed by a drop detection algorithm based on Young-Laplace equation (One Attension software). The accuracy of the algorithms is argued to be of the order of ± 0.1º (*e.g.* [27]). Contact angle hysteresis was assessed at room temperature as described by Kietzig [28]. Briefly, a small water drop is dispensed from a needle and brought into contact with the surface. The volume of the drop is increased and the advancing contact angle is taken as the one just before the interface diameter increases. Afterwards, the drop diameter is decreased and the receding contact angle is taken as the one just before the interface diameter decreases [28].

Then, complementary information is given by the spreading diameter, which is obtained from high-speed visualization and post-processing. The high-speed images were taken at 2200fps using a Phantom v4.2 from Vision Research Inc.,

with 512x512pixels@2100fps resolution and a maximum frame rate of 90kfps. For the present optical configuration the spatial resolution is 25pixel/μm and the temporal resolution is 0.45ms.

The spreading diameter is evaluated based on a home made post-processing routine developed in Matlab. The spreading diameter measured with and without electrostatic actuation is averaged over 6 events, obtained at similar experimental conditions. Accuracy of the measurements is evaluated to be ±25μm. Regarding initial droplet diameters and impact velocities, the accuracy in the evaluation of the impact droplet diameter is ±1.4%, while for the velocity it is better than 3%.

Non-Newtonian behaviour of the fluids

As further discussed in the following section, a non-Newtonian (shear-thinning) behaviour was only observed for the droplets of water+xanthan gum mixtures. The viscosity vs shear rate curves were fitted using the Cross model [29]:

$$\frac{\eta_{eff} - \eta_\infty}{\eta_0 - \eta_\infty} = \frac{1}{1 + (C\dot{\gamma})^m} \quad (1)$$

being η_{eff}, η_0 and η_∞ the effective, zero-shear (upper limit) and infinite-shear (lower limit) viscosities, respectively. *C* is the Cross time constant and *m=1-n*. Thus, as *m* increases, the mixture becomes more shear-thinning.

The fitting parameters are given in Table 2, together with the main physico-chemical properties of the mixtures, taken at ambient temperature and pressure. The rheological data was measured at controlled temperature conditions, at ATS RheoSystems (a division of CANNON® Instruments, Co). The accuracy of the data is within ±5%. In the table, X stands for xanthan and the percentage following is the wt% of xanthan gum in the mixture with water. It is worth mentioning that except for the viscosity, all the other properties of the xanthan gum solutions are very close to those of water. All the other fluids depict a Newtonian behaviour, with liquid viscosity and surface tension values also close to those of water.

As for the biological fluids and NaCl solutions, the density, surface tension and viscosity are all also close to that of water ($1.0013<\rho<1.002$kg/m^3, $70.92<\sigma_{lv}<73.83$x10^{3}N/m and $\eta_0 \approx 8.9$x10^{-4}Pa.s). Nevertheless, to assure that any of these solutions depict non-Newtonian flowing behaviour, droplet dynamics without electrostatic actuation is briefly assessed as further discussed in the results.

Table 2. Thermophysical properties of the working fluids taken at 20ºC. Here X stands for xanthan and the percentage following is the wt% of xanthan gum in the mixture with water.

Fluid	ρ [kg/m^3]	σ_{lv} [N/m]x10^3	η_0 [Pa.s]	η_∞ [Pa.s]	C [s]	m [-]
Water	996	72.75	8.9x10^{-4}	8.9x10^{-4}	-	-
X0.05%	997	73.00	0.08	1.9	0.8	0.678
X0.10%	997	72.00	0.22	2.6	1.3	0.696
X0.15%	997	71.50	0.58	3.6	1.65	0.707
X0.35%	997	72.95	13.29	5.1	13.97	0.804

Electrowetting configuration

The electrostatic actuation is performed in a single-plate configuration, following the schematics presented in Figure 2.

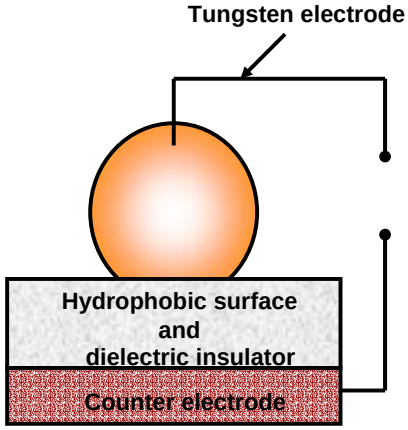

Figure 2. Schematic showing the configuration used for the electrowetting actuation experiments.

A 10μm Teflon film is used as the dielectric under the micro-structured surfaces. As recommended by Restolho *et al.* [30] a very thin film of sodium chloride was placed between the counter electrode and the dielectric to avoid the presence of an air gap.

The electrode dipped inside the droplet is a tungsten wire with 0.025mm diameter (Goodfellow Cambridge Ltd). The counter electrode is a copper cylinder. Both electrodes were connected to a Sorensen DCR600-.75B power supply and DC voltage is applied in increments of 25V. Reversibility measurements are performed decreasing the voltage from the maximum value down to 0V, also in steps of 25V. Although AC voltage is reported by some authors to lead to better performances of the electrowetting systems (*e.g.* [10]) one used DC voltage since the purpose of this work is to extrapolate some of these results to develop a test chip that may overcome the limiting frequencies for which the conditions for which Lippmann equation is valid are not satisfied [8]. At least 6 tests are performed to obtain an average curve (contact angle *vs.* applied voltage). An illustrative curve obtained for NaCl (100mM) is depicted in Figure 3.

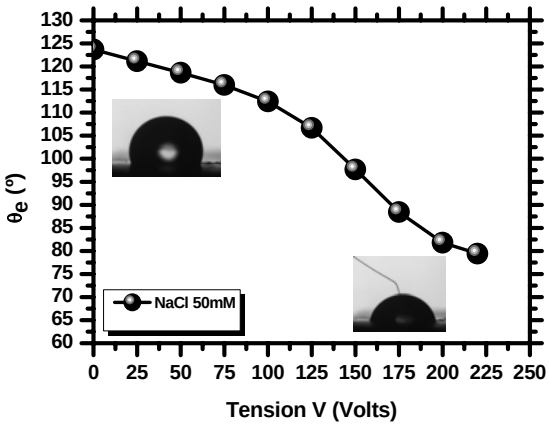

Figure 3. Illustrative curve of the contact angle as a function of the applied voltage, taken with a 3μL droplet of NaCl (100mM).

Viability tests

After the electrostatic actuation one must infer if the samples suffered significant modifications and if they are still viable. For the biological fluids used here, a major concern is the stability of the BSA protein, as this may denature due to the electrostatic actuation. This was checked by measuring the absorption spectra of the BSA solutions before

and after the actuation experiments using a NanoDrop 2000c/2000 UV-Vis spectrophotometer (Thermo Scientific). The scans were performed in the 250-400 nm wavelength range using 2 ul of solutions.

Results and Discussion

Static and dynamic wetting without electrostatic actuation

Table 3 summarizes the static angles for each of the liquid-surface pairs considered here. From a total of 15 tested surfaces, only those depicted in the table kept hydrophobic angles (over 100º) for all the liquids tested. The experiments performed also show no significant effect of varying the concentrations of NaCl or protein (BSA) in the solutions, so that only the results obtained for one illustrative concentration are depicted here. It is worth mentioning that although the static angles are overall quite high, only surface S5 rendered hystreresis of the order of 10º for the various liquids tested (i.e. the surface has superhydrophobic properties). This can be a problem during electrostatic actuation since it may preclude the occurrence of reversibility. To further investigate this issue and before submitting the samples to electrostatic actuation, forced droplet spreading was further characterized, by impacting the droplets on the surfaces at low velocities. The temporal evolution of the resulting contact diameter is depicted in Figure 4. In order to avoid an exhaustive description, results are only presented here for the spreading of plasma mock over surfaces S1, S2, S3 and S5. Given that the hysteresis is significantly high for most of these surfaces, pinning of the contact line may occur on the micro-patterns. Consequently, energy is dissipated at the contact line, so that a smaller spreading diameter of the droplets is observed over these surfaces. Also, the recoiling is lessened, thus suggesting that one will have an electrowetting induced irreversible motion over these surfaces. A similar trend was observed for all the other surfaces, including the PTFE surface.

Table 3. Equilibrium contact angles for the representative pairs liquid-surface used in the present work.

	Water	NaCl (100mM)	Plasma mock
S9	127	129.7	122
S10	140	143.7	144.9
S14	115.6	111	118
SHS	152.4	148.4	150
PTFE	112	112.2	112.4

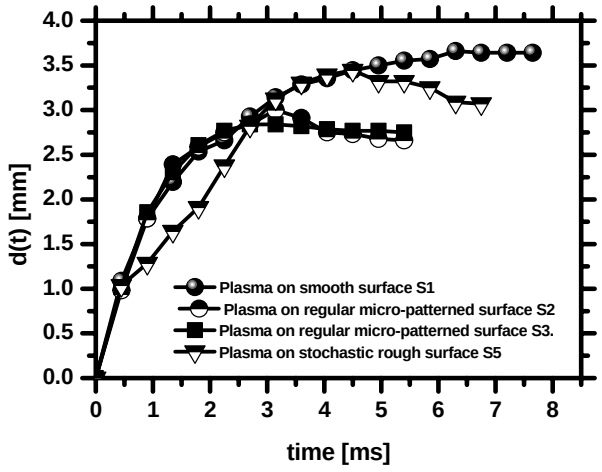

Figure 4. Spreading of a plasma mock droplet D_0=3.2mm, U_0=0.44m/s over various surfaces without electrostatic actuation.

Non-Newtonian behaviour of the droplets

In agreement with the preliminary rheological analysis of the biological liquids, reported in the section of Materials and methods, the spreading morphology of these fluids does not depict any evident non-Newtonian behaviour. The maximum spreading diameters of plasma mock and DNA droplets are further made dimensionless with the initial droplet diameter and are compared, in Figure 5, to the maximum spreading diameter of a Newtonian (water) and of non-Newtonian (water+xanthan mixtures) droplets, previous obtained in [31] and with the predictions of the Roisman *et al.* model [32].

This model was selected, as it was observed to be well fitted to a wide range of experimental impact conditions for Newtonian droplets, as reported in [31]. The reason for this good agreement is associated to a variable scaling of the viscous dissipation term in the energy balance, depending on the relative importance of this term in the spreading.

The results depicted in Figure 5 show that the experimental data obtained for plasma mock and DNA droplets are closer to those obtained for water and much apart from those obtained with water+xathan mixture (035%wt), which has a strong non-Newtonian spreading behaviour. The differences observed between water when compared to the plasma mock and DNA data can be attributed to wetting differences due to the slight variation of the surface tension in the biological fluids.

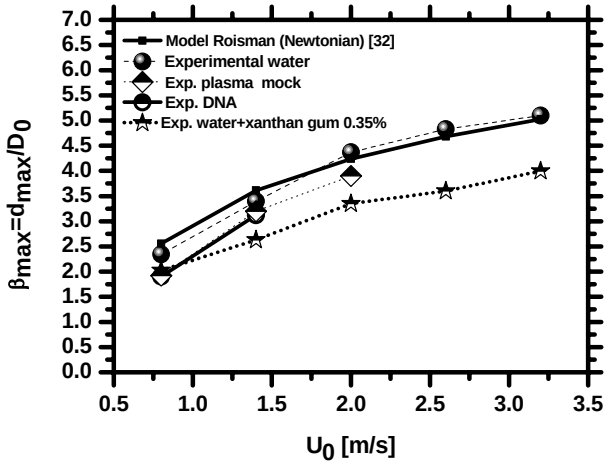

Figure 5. Characterization of possible non-Newtonian behavior of the DNA and plasma mock droplets by comparison with theoretical predictions of the spreading ratio $\beta_{max}=d_{max}/D_0$ and with other experimental results previously obtained in [31] with water+xanthan gum mixture droplets. All the droplets have a D_0=3.2mm and impact on a smooth silicon surface at room temperature.

Static and dynamic wetting with electrostatic actuation

Droplet spreading induced by electrowetting was investigated for static and dynamic conditions. For static conditions the droplets were deposited on the substrates and actuated with gradually increasing voltage. For illustrative purposes, only the results with the PTFE substrate are shown as the surface is representative in terms of the static wetting effects as aforementioned, but one has not to deal with the additional effect of the regular micro-pattern, which requires deeper investigation.

In line with this, Figure 6 depicts the equilibrium contact angle as a function of the applied voltage for NaCl, blood plasma mock and BSA for different concentrations.

The results in the figure suggest a mild effect of the concentration for the various solutions. Hence, for NaCl, electrowetting is slightly enhanced (i.e. the contact angle decreases more with the applied voltage and this decrease is observed from lower values of the voltage) as the concentration increases from 50mM to 200mM. Then, electrowetting induced decrease of the contact angle becomes again less efficient for concentrations of 400mM. This suggests an optimum concentration around 100mM for the conditions tested here. Most of the authors (*e.g.* [12,33]) report an insignificant effect of the concentration of NaCl on the electrowetting-induced decrease of the contact angle. However these authors usually work with smaller droplets and lower salt concentrations. Also, [34] found an effect of pH and [8] suggest a possible modification of the electrical fields due to adsorption of the salts by the dielectric substrate which may in turn affect the electrowetting. The contact angle of the BSA solutions seem to be more difficult to decrease at lower actuation voltages, but shows a steeper slope for higher voltages, which suggests that the BSA transport is also promoted by small increases of its concentration. This may be also explained by the adsorption of the protein by the dielectric substrate, which affects the electrical field near the contact line, as BSA is negatively charged

at the pH of the experiment. Hence, the relatively high saturation angle (about 80º) observed for the BSA solutions can be actually due to the time that the droplet is deposited over the surface that promotes the adsorption of the molecules and locally changes the wettability, lowering the contact angle and making the motion of the contact line more difficult for the latest parts of the test, which correspond to the highest actuation voltage.
It is worth mentioning that the induced advance of the contact line was observed to be irreversible for all the electrwetting tests performed.
Additional information was obtained by observing the transient morphology of the actuated droplets, by high-speed visualization. In this case a new droplet is used for each droplet, to infer if the motion of the contact line was being influenced by the irreversibility caused by the decrease of the contact angle. Qualitative analysis of the high-speed videos (not shown here) evidences the occurrence of asymmetry in the shape of the droplet due to hysteresis. Also, in some cases the hysteresis leads so significant differences in the motion of the contact line that actually induce the slip of the droplet in the opposite direction.
Considering now a more quantitative analysis, Figure 7 shows the temporal evolution of the electrowetting induced spreading of the contact line, for the concentrations reported in Figure 6. t=0 corresponds to the time instant when the droplet is actuated. The curves obtained here are qualitatively in agreement with those reported by [23], exception made to the fact that our curves depict more oscillations. This maybe attributed to the high temporal resolution used here, which is larger than the velocity of contact line.

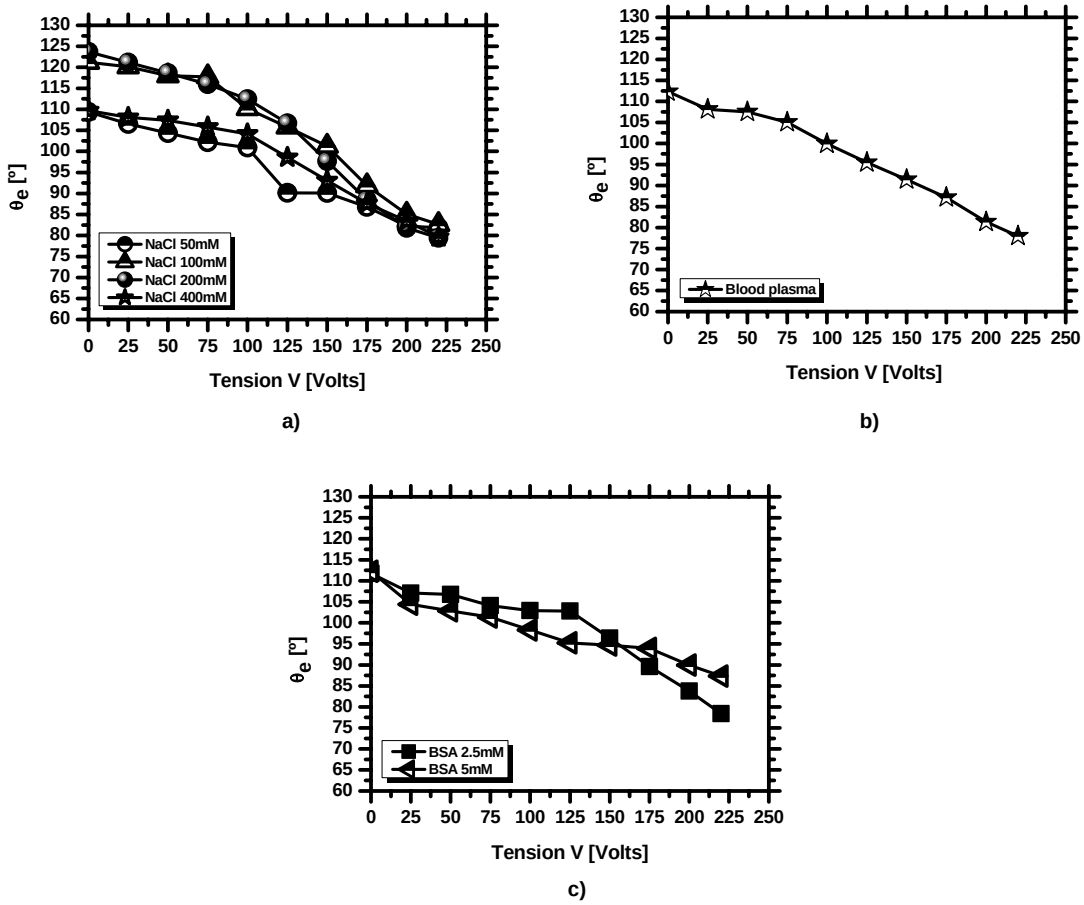

Figure 6. Contact angle as a function of the applied voltage for solutions of **a)** NaCl, **b)** plasma mock and **c)** BSA, for different concentration of the solutions. The droplets have an initial diameter D_0=2.4mm.

Overall the spreading diameter is in agreement with the trends suggested in Figure 6, given that the electrowetting seems to be slightly promoted by the increase of the concentration. Here, the difficulty in the transport of the protein is not so clear, as the highest concentration BSA solution actually depicts one of the largest spreading diameters for the highest actuation voltage. Hence, the apparent limitation in droplet motion suggested in the static analysis for the solutions with higher concentration of BSA may be indeed related to local wetting modifications resulting from the long period that is available for adsorption of the molecules by the dielectric substrate.

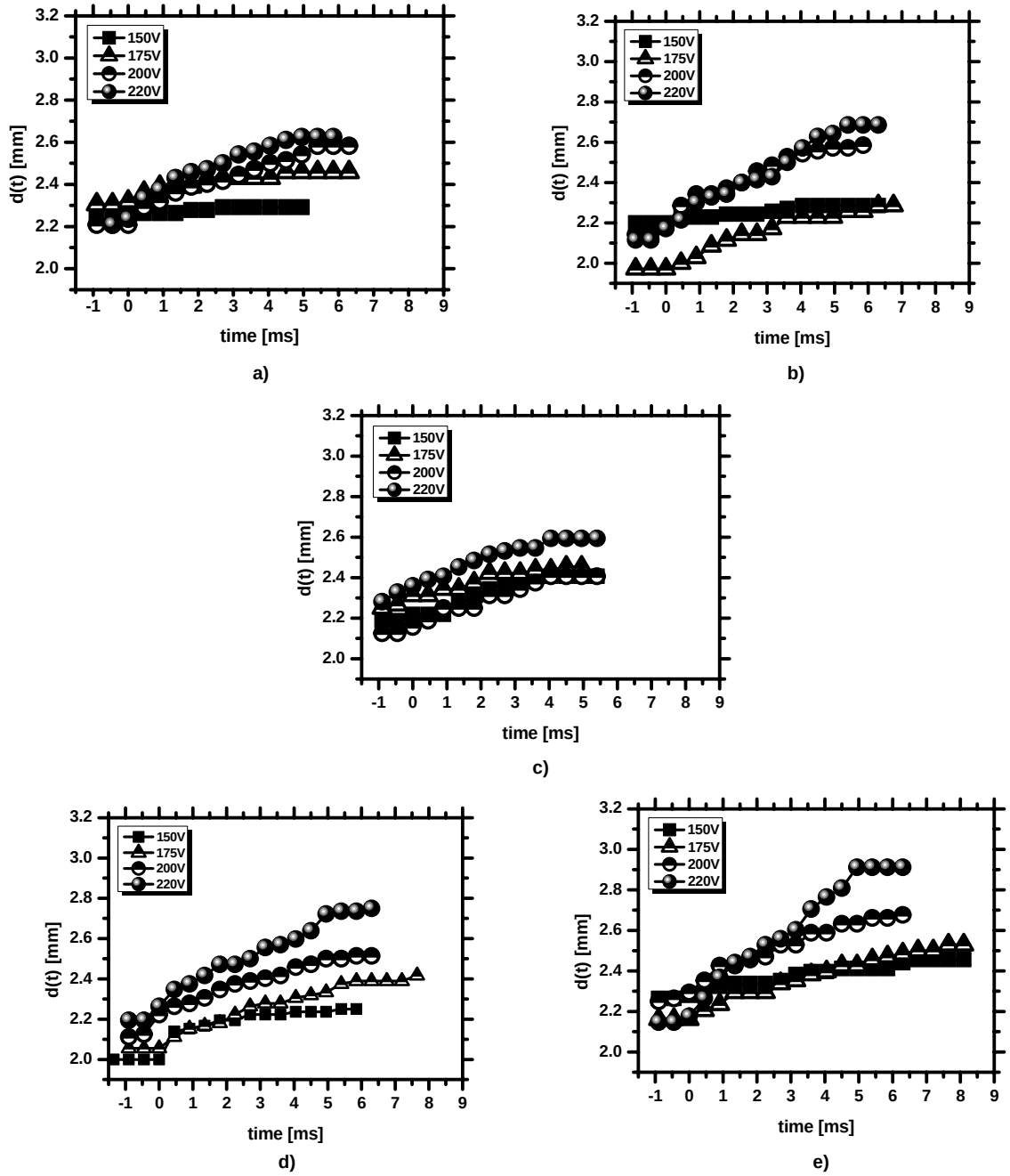

Figure 7. Electrowetting induced spreading of the contact line for solutions of **a)** NaCl (50mM), **b)** NaCl (100mM), **c)** plasma mock, **d)** BSA (1mM) and **e)** BSA (2.5mM). The droplets have an initial diameter D_0=2.4mm.

Viability of the samples

The impact of electrostatic actuation on the stability of BSA was inferred by comparing the absorption spectra of the solutions before and after actuation. The tests were performed for the solutions with the lowest and highest concentrations of 1mM and 50mM, respectively. The obtained spectra, shown in Figure 8 reveal that BSA does not suffer any structural modification, as the spectra obtained before and after electrostatic actuation are similar. The increase in the absorption peak observed at 50mM concentration after electrowetting is ascribed to droplet evaporation, which leads to an increase in the concentration of 1.5times. This increase in the concentration is estimated to be indicative of a decrease in the volume of the droplet by evaporation of approximately 30%.

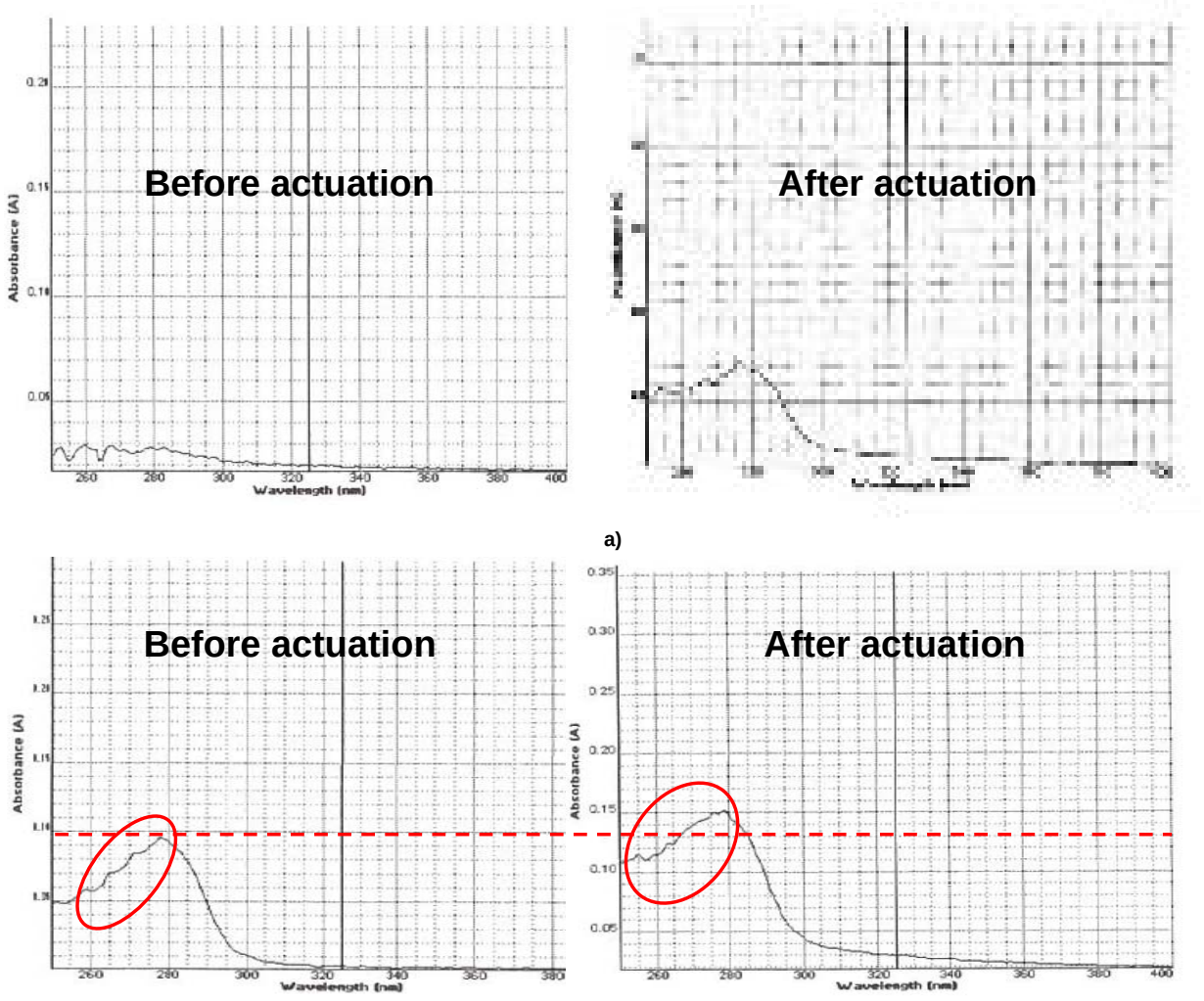

Figure 8. Absorption spectra obtained for the BSA solutions with **a)** 1mM and **b)** 50mM concentration before and after electrowetting.

To assure that droplet evaporation is actually caused by electrowetting and not by mass diffusion to the surrounding air, the absorption spectra were repeated on the samples by simply depositing the droplets over the substrate and waiting the time period that was required to complete tests with electrostatic actuation. The results, as depicted in Figure 9 confirm that the evaporation of the droplet is indeed caused by electrowetting. This maybe a problem for applications in lab-on-a-chip devices, particularly for diagnostic purposes which rely on the detection of the protein (or any other component transported in the droplet) and therefore deserves more attention in future studies.

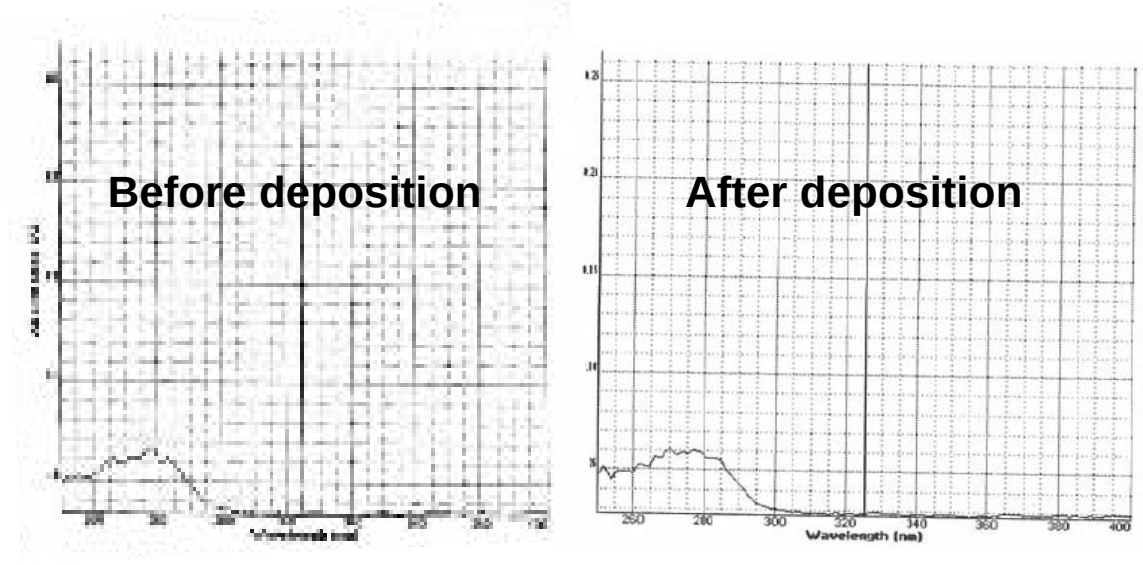

a) **b)**

Figure 9. Absorption spectra obtained for a BSA solution (50mM) without electrostatic actuation. **a)** Spectrum of the original solution, **b)** spectrum of solution after deposition on the surface during the time period required for completion of the electrowetting tests.

Final Remarks

The present paper addresses the forced spreading of biological droplets over enhanced surfaces with and without electrostatic actuation, in the context of sample handling in lab-on-a-chip applications. The best performing enhanced surfaces are chosen based on the characterization of wettability (static and dynamic contact angles) and on the analysis of droplet impact at small velocities. The tests consider the use 2-3mL droplets of NaCl, plasma mock (100mmol/l NaCl, 1.2mmol/l BSA, 5.6mmol/l glucose) and BSA solutions with different concentrations.

Droplet spreading induced by electrowetting was investigated for static and dynamic conditions.

The results show a mild effect of the concentration of the salt and of the protein in promoting droplet motion by electrowetting. The static analysis of the electrowetting (based on the gradual evolution of the equilibrium angles) showed however a relatively high saturation angle for the BSA solutions, which limited the droplet motion at the highest actuation voltage. This information was however complemented with the dynamic analysis of the contact line motion (inducing droplet spreading) under electrostatic actuation), which refutes this trend showing large spreading of the contact line of BSA solutions, when actuated by the highest voltage. Hence, the apparent high saturation angle can be attributed to the adsorption of the molecules by the dielectric substrate, which may induce modifications of the wettability, if the droplet stays in contact with the dielectric for enough time.

Analysis of the absorption spectra of the samples before and after electrowetting reveals that the samples remain unchanged after electrostatic actuation, but that the transport droplet evaporates, causing an increase of the concentration of the biological sample.

Acknowledgements

The authors are grateful to Fundação para a Ciência e a Tecnologia (FCT) for partially financing the research under the framework of project PTDC/EME-MFE/109933/2009), which also supports J. A. Ramos with a fellowship. The work was also partially financed by FCT through the project RECI/EMS-SIS/0147/2012. A.S. Moita also acknowledges the contribution of FCT for Post-Doc Fellowship (Ref.:SFRH/BPD/63788/2009). Finally the authors would like to thank Professor J. L. Mata for his valuable help in setting up the electrowetting configuration.

References

[1] Hong, L. and Pan, T., 2011, Microfluid. Nanofluid, 10, pp. 991–997.

[2] Park, J.K.,Seung, J.L. and Kang, K.H., 2010, Biomicrofluidics, 4, pp. 024102.

[3] Manz, A. abnd Becker, H., 1998, Microsystem Technology in Chemistry and Life Science (Srpinger Topics in Current Chemistry, 154.
[4] Jakeway, S.C., de Mello, A.J. and Russel, E.L., 200, J. Anal. Chem., 355, pp. 525.
[5] Hong, J.W. and Quake, S.R., 2003, Nat. Biotechnol. 21, pp. 1179.
[6] Barbulovic-Nad, I., Yang, H., Park, P.S. and Wheeler, A. R., 2008, Lab Chip, 8, pp. 519-526.
[7] Mohamed, H., Turner, J. N. and Caggana, M., 2007, J. Chromatography A, 1162, pp. 187-192.
[8] Muegle, F. and Baret, J.-C., 2005, J. Phys.: Condens.Matter, 17, pp. R705-R774.
[9] Cooney, C.G., Chen, C.-Y., Emerling, R., Nadim, A. and Sterling, J. D., 2006, Microfluid Nanofluid, 2, pp. 435-446.
[10] Jones, T.B., 2005, J. Micromechanics and Microengineeering, 15, pp. 1184-1187.
[11] Pollack, M.G., Pamula, V.K., Srinivasan, V. and Eckhardt, A.E., 2011, Expert Review of Molecular Diagnostics, 11(4), pp.397-407.
[12] Berge, B., 1993, C. R. Acad. Sci, II, 317, pp. 157.
[13] Kuo, J.S., Spicar-Mihalic, P., Rodriguez, I. And Chiu, D., 2003, Langmuir, 19, pp. 250.-255.
[14] Bahadur, V. and Garimella, S.V., 2006, J. Micromechanics and Microengineeering, 16, pp. 1494-1503.
[15] Srinivasan, V., Pamula, V.K. and Fair, R.B., 2004, Lab Chip, 4, pp. 310.
[16] Srinivasan, V., Pamula, V.K. and Fair, R.B., 2004, Appl. Phys. Lett., 82, pp. 4187.
[17] Yoon, J.Y. and Garrell, R.L., 2003, Anal. Chem., 75, pp. 5097.
[18] Wheeler, A.R., Moon, H., Kim, C.J., Loo, J. and Garrell, R.L., 2004, Anal. Chem., 76, pp. 4833.
[19] Sharma, K. and Bhat, S.V., 1992, Phys. Chemistry and Physics and Medical NMR, 24(4), pp. 307-312.
[20] Brust, M., Schaefer, C., Doerr, R., Pan, L., Arratia, P.E. and Wagner, C., 2013, Phys. Rev. Lett., 110, pp. 078305.
[21] Robins, Trans. Faraday Soc., 1964, 60, pp. 1344-1351.
[22] Moita, A.S., Herrmann, D. And Moreira, A.L.N., Sept. 1-4 2013, 25th European Conference on Liquid Atomization and Spray Systems, Chania, Greece.
[23] Annapragada, S.R., Dash, S., Garimella, S.V. And Murthy, J.Y., 2011, Langmuir, 27(8), pp. 8198-8204.
[24] Moita, A.S. and Moreira, A.L.N., 2007, Int. J. Heat Fluid Flow, 28, pp. 735-52.
[25] Moreira, A.L.N., Moita, A.S. and Panão, M.R., 2010, Progress in Energy and Combustion Science, 36, pp. 554-80.
[26] Rioboo R, Tropea C. and Marengo M., 2002, Atom. and Sprays, 11, pp. 155-65.
[27] Cheng P., 2008, PhD Thesis, University of Toronto, Canada.
[28] Kietzig AM., 2008, Plasma Processes and Polymers, 8, pp.1003-1009.
[29] Cross, M.M., 1965, J. Colloid Sci., 20, pp.417-437.
[30] Restolho, J., Mata, J.L. and Saramago, B., 2009, Langmuir, 113, pp. 9321-9327.
[31] Moita, A.S., Herrmann, D. and Moreira, A.L.N., 2014, Applied Thermal Eng.
[32] Roisman, I. V., Berberovic E. and Tropea, C.,2009, Phys. Fluids, 21(5), pp. 052103.
[32] Verheijen, H.J.J. and Prins, M.W.J., 1999, Langmuir, 15, pp. 6616.
[34] Quinn, A., Sdev, R. And Ralston, J., 2003, J. Phys. Chem. B., 107, pp. 1163.